The presence of O_2 at F-layer altitudes should have a profound effect on the rate of electron recombination as suggested by Bates and Massey.[10] Since atomic oxygen ions can be converted to molecular ions in collisions with neutral oxygen molecules, the molecular ions can then recombine with electrons by dissociative recombination,

$$e+O_2^+ \rightarrow O'+O''. \quad (2)$$

The recombination coefficient for this process may be as large as 10^{-7} cm^3 sec^{-1}. By contrast, in the absence of molecular oxygen, electron recombination proceeds by radiative recombination,

$$e+O^+ \rightarrow O+h\nu, \quad (3)$$

for which the recombination coefficient is of the order of 10^{-12} cm^3 sec^{-1}. Since the conversion of atomic to molecular ions,

$$O^+ + O_2 \rightarrow O_2^+ + O, \quad (4)$$

can take place by either charge exchange or by ion-atom interchange, a large reaction cross section is expected. According to Bates,[11] the rate coefficient for ion-atom interchange may be as high as 10^{-10} cm^3 sec^{-1}. The high-altitude O_2 concentrations indicated by the rocket experiment and the theoretical cross section for exchange ionization are sufficient to explain the recombination coefficients of 10^{-10} to 10^{-9} observed in F_2 region.[12] The manner in which the recombination coefficient decreases from E region to F_2 region depends on the partial pressure of O_2. The expected rate of decrease is sufficient to account for the production of a major portion of F_2 region by the same source of ionization that is responsible for F_1.[12,13]

[10] D. R. Bates and H. S. W. Massey, Proc. Roy. Soc. (London) **A192**, 1 (1947).

[11] D. R. Bates, Proc. Phys. Soc. (London) (to be published).

[12] Havens, Friedman, and Hulburt, Report of the Conference on the Physics of the Ionosphere, The Physical Society, London (1954).

[13] N. Bradbury, Terrestrial Magnetism and Atm. Elec. **43**, 55 (1938).

PHYSICAL REVIEW VOLUME 98, NUMBER 6 JUNE 15, 1955

Theory of Electron Penetration*

L. V. SPENCER
National Bureau of Standards, Washington, D. C.

(Received January 20, 1955)

The theory of electron penetration in an infinite medium under the combined influence of scattering and slowing down is developed to the point of numerical application. Sample calculations of energy dissipation *versus* distance from the source are compared with experiments by Frantz, by Clark, Brar, and Marinelli, and by Loevinger. The agreement is good provided that relativistic scattering cross sections are used. The energy loss is treated in the continuous slowing down approximation; the resulting error is appreciable only at extreme penetrations.

1. INTRODUCTION

THIS paper considers the following problem: A source of electrons with kinetic energy T_0 is embedded in a material. As the electrons move away from the source they lose energy and change direction. We want to determine the energy dissipated by the electrons at various locations in the material. A knowledge of the distribution of energy dissipation implies a knowledge of the spectral and directional distributions also, but this additional information need not be described explicitly.

Phenomenological work on this problem has been accomplished mainly by people interested in the biological effects of radiation. The most extensive effort of this type, and also the most recent, is that of Loevinger, whose paper contains a fairly complete summary of experimental work with beta-ray sources.[1] From a more basic standpoint the problem is essentially new, since few attempts—and those in unrealistic schematization—have been made to calculate electron spatial distributions taking into account both energy loss and direction changes, although both effects have a strong influence.[2,3] Many contributions have been made to-

* Work supported by the U. S. Atomic Energy Commission and the Office of Naval Research.

[1] R. Loevinger (private communication).

[2] For efforts to apply age diffusion theory to electron penetration problems see Bethe, Rose, and Smith, Proc. Am. Phil. Soc. **78**, 573 (1938) and W. C. Roesch, Hanford Report No. HW-32121, May 24, 1954 (unpublished). There can be hardly any doubt that this simple model gives better than an order-of-magnitude estimate of the distance electrons travel "on the average." However, two important features of the penetration are given wrongly: (a) The initial transient stage of the penetration when electrons move directly away from the source, which is particularly important for high-energy sources or for low-Z scattering materials; and (b) the deep-penetration trend. The results of this paper indicate that there is hardly any region of penetration in which age diffusion theory can be expected to provide a reasonable description.

[3] For calculations of electron backscattering see J. W. Weymouth, Phys. Rev. **84**, 766 (1951). Weymouth took into account energy losses as well as deflections, but only in the approximation of an energy-independent scattering cross section. He did not attempt to calculate electron spatial distributions.

wards understanding simpler situations, in which one or another effect is neglected. For example, many authors have neglected angular deflections in calculating spatial distributions as a function of energy loss.[4] This is the so-called straggling problem. Other authors have neglected energy loss effects in calculating angular distributions produced by penetration.[5] In addition, there has been work relating the deflections to energy losses neglecting the spatial dependence[6] and some work on energy losses neglecting *both* direction and spatial location.[7] A discussion of these partial problems together with their inter-relationships is given in the first part of Fano's paper on straggling and energy loss of charged particles.[8]

H. W. Lewis took the first step towards a more realistic theoretical treatment of the electron penetration when he wrote down formal expressions for the spatial moments of the electron distribution.[9] These were based on a continuous energy loss approximation. Both elastic and inelastic deflections were included in his derivation, the latter being considered as statistically independent of the energy losses. Lewis made no attempt to evaluate the moments numerically in a systematic way or to use them to obtain spatial distributions.

Following the publication of Lewis' paper, evaluation of a limited number of moments was accomplished in nonrelativistic approximation by Blanchard.[10] Blanchard also found very useful approximate expressions for the harmonic coefficients of the zeroth spatial moment, which have special interest.[6] Attempts were then made by Blanchard and others to construct spatial distributions from a knowledge of the first few moments.[10] The results were generally unsatisfactory, because the information contained in the first few moments did not seem sufficient for such a construction.

The essential information which was lacking in this earlier work was a knowledge of the asymptotic (deep-penetration) trend. Although complete knowledge of the spatial moments theoretically should yield the distribution, in practice it is not possible to calculate more than a finite, comparatively small number of spatial moments and these with imperfect accuracy. Construction of a spatial distribution is equivalent to extrapolating this finite set of imperfectly known moments to infinite order. Unless the trend of the high-order spatial moments is known from a determination of the deep-penetration spatial trend, such an extrapolation cannot be made with confidence.

Several developments have now made it possible to calculate realistic electron spatial distributions at least for situations in which bremsstrahlung energy losses may be neglected. First, methods were developed for rapid desk-computer calculation of large numbers of spatial moments. When numerical values for the moments were graphed, they showed very clearly the trend predicted by a Wick-type asymptotic calculation,[11] so much so that the high moments seemed to contribute little additional information. This "break" made spatial distribution constructions feasible. Next, methods had to be found for combining into an analytic form (a) the known values of a number of spatial moments, (b) the asymptotic trend, and (c) additional odds and ends of information about the distribution. This was not easy, because traditional methods did not seem to work. Eventually "function-fitting" techniques were developed similar to those which have proved useful in x-ray penetration problems,[12] and satisfactory constructions were made. Finally, a much better theoretical derivation of the all-important deep-penetration trend was discovered which removed remaining questions about its reliability and range of application.

The methods for calculating spatial moments are described in Secs. 2, 3, and 4. The deep-penetration trend is then considered (Sec. 5), but only in connection with a Wick-type argument (Appendix D) since the newer derivation will be presented in a later paper. Additional information which must be used in constructing distributions is given in Sec. 6. All the presentation up to this point deals explicitly with plane monodirectional and monoenergetic electron sources because they are easily visualized, although the principles apply to other types as well. The remaining sections contain material about several source types. The actual construction of distributions is discussed in Secs. 7 and 8. In Sec. 9 there are several examples of calculations in plane monodirectional geometry. These are compared with experiments by Frantz [see Sec. 9(B)]. In Sec. 10

[4] See L. Landau, J. Phys. (U.S.S.R.) **8**, 201 (1944); O. Blunck and S. Leisegang, Z. Physik **128**, 500 (1950); also, for heavy particles, K. R. Symon, Harvard thesis, 1948 (unpublished) whose results are extensively quoted by B. Rossi, *High Energy Particles* (Prentice-Hall Inc., New York, 1952), pp. 29 ff.

[5] E. J. Williams, Proc. Roy. Soc. (London) **169**, 531 (1939); S. Goudsmit and J. L. Saunderson, Phys. Rev. **57**, 24 (1940); G. Molière, Z. Naturforsch. **32**, 78 (1948); H. S. Snyder and W. T. Scott, Phys. Rev. **76**, 220 (1949); H. A. Bethe, Phys. Rev. **89**, 1256 (1953); and L. V. Spencer, Phys. Rev. **90**, 146 (1953). Also of this type but emphasizing mainly the backscattering are papers by W. Bothe, Z. Physik **54**, 161 (1929); Bethe, Rose, and Smith, Proc. Am. Phil. Soc. **78**, 573 (1938); M. C. Wang and E. Guth, Phys. Rev. **84**, 1092 (1951); T. Teichman, Atomic Energy Commission Document NYO-785, 1951 (unpublished); and E. J. Saletan, Atomic Energy Commission Document NYO-3990, 1952 (unpublished).

[6] C. H. Blanchard, National Bureau of Standards Circular 527, 1954, p. 9. Note that with the continuous energy loss approximation, which relates path length to energy loss, most of the papers of the preceding footnote can be considered in this category also.

[7] L. V. Spencer and U. Fano, Phys. Rev. **93**, 1172 (1954).

[8] U. Fano, Phys. Rev. **92**, 328 (1953).

[9] H. W. Lewis, Phys. Rev. **78**, 526 (1950).

[10] C. H. Blanchard (private communication).

[11] G. C. Wick, Phys. Rev. **75**, 738 (1949). This type of analysis was first applied to an electron penetration problem by Yang [C. N. Yang, Phys. Rev. **84**, 599 (1951)]. He derived the path length distribution for a fixed and small penetration. We seek the related penetration distribution for a fixed path length. Yang's limitation to small energy loss makes the Wick-type analysis much more straightforward than in the general case.

[12] L. V. Spencer, Phys. Rev. **88**, 793 (1952).

there are sample calculations for point and plane isotropic P^{32} sources which are compared with experiments by Clark, Brar, and Marinelli and by Loevinger.[1] In all comparisons, theory and experiment agree to perhaps three percent or better except where extraneous effects are to be expected. These extraneous effects are range straggling, which has not been included in the calculations and which becomes important at the very deepest penetrations, and a boundary at the source plane which is present in Frantz's experiment.

The remarks at the end are mainly concerned with methods for extending the theory to more general situations and including effects neglected in this treatment.

2. THE TRANSPORT EQUATION

Our presentation relates chiefly to monoenergetic and monodirectional sources which are distributed uniformly over an infinite plane and to scattering media which are homogeneous and without boundaries.[13] The use of monoenergetic sources is not a limitation since problems involving polychromatic sources can be solved by simple integration over monoenergetic source results. The consideration of only plane monodirectional geometry is likewise not particularly a limitation. Other simple geometries can be treated in the same way.[14] In particular, it is easily possible to convert a solution for a *plane isotropic* source into a solution for a *point isotropic* source. This conversion is discussed in Sec. 8.

If an electron source located at the plane $z=0$ emits monoenergetic electrons in the direction $\theta=0$ perpendicular to the source plane, Lewis' equation[9] describing the penetration may be written as follows:

$$-\frac{\partial I}{\partial r}+\cos\theta\frac{\partial I}{\partial z}=\int d\Omega' N\sigma(r,\Theta)\{I(r,\theta',z)-I(r,\theta,z)\}+(2\pi)^{-1}\delta(z)\delta(r-r_0)\delta(\cos\theta-1). \quad (1)$$

Here, $2\pi I(r,\theta,z)\sin\theta d\theta dr$ is the *flux* of electrons, with obliquities between θ and $\theta+d\theta$ and with residual ranges between r and $r+dr$, crossing the surface of a unit spherical probe located a distance z from the source plane. Likewise, $2\pi\sigma(r,\Theta)\sin\Theta d\Theta$ is the cross section per atom for deflecting an electron with residual range r through an angle of a size between Θ and $\Theta+d\Theta$, while N is the number of atoms per gram of material. The term on the right containing the Dirac delta functions specifies the electron source.[15]

By assuming that the electrons lose their energy continuously, a relation is established between the residual true range r and the kinetic energy of the electrons. The average rate of energy loss is the stopping power (dT/dr), for which theoretical expressions exist.[16] The connection between r and T is given by the following integral over the stopping power:

$$r(T)=\int_0^T dT(dT/dr)^{-1}. \quad (2)$$

Table I gives electron ranges which have been calculated numerically by integrating over stopping powers determined from the Bethe formula. Note that throughout this paper T expresses kinetic energy in mc^2 units while r is measured in g/cm^2.

At this point it is convenient to rescale the distance parameters, taking $r_0=r(T_0)$ as a unit. Defining $t=(r/r_0)$, $x=(z/r_0)$, $S(t,\Theta)=r_0N\sigma(r,\Theta)$, and $I(r,\theta,z)dr=I(t,\theta,x)dt$, the transport equation takes the form

$$-\frac{\partial I}{\partial t}+\cos\theta\frac{\partial I}{\partial x}=\int d\Omega' S(t,\Theta)\{I(t,\theta',x)-I(t,\theta,x)\}+(2\pi)^{-1}\delta(x)\delta(t-1)\delta(\cos\theta-1), \quad (3)$$

where the dimensionless energy parameter t varies from 0 to 1, while the space parameter x varies from -1 to $+1$.

The first step in treating this complicated equation is an expansion in spherical harmonics, which is easily performed with the aid of the well-known addition theorem. Defining

$$I_l(t,x)=2\pi\int_{-1}^{1}d(\cos\theta)P_l(\cos\theta)I(t,\theta,x),$$
$$S_l(t)=2\pi\int_{-1}^{1}d(\cos\Theta)\{1-P_l(\cos\Theta)\}S(t,\Theta), \quad (4)$$

Eq. (3) may be transformed to a linked system of differential equations:

$$-\frac{\partial I_l}{\partial t}+(2l+1)^{-1}\left\{(l+1)\frac{\partial I_{l+1}}{\partial x}+l\frac{\partial I_{l-1}}{\partial x}\right\}+S_l(t)I_l(t,x)=\delta(x)\delta(t-1). \quad (5)$$

The second step is a transformation in terms of spatial moments. The Eqs. (5) are multiplied by different powers of x and integrated over the whole range $-1<x<+1$. The resulting system of equations is the

[13] The calculation of boundary effects, even for the simplest geometries, is an unsolved problem. As mentioned in references 2 and 3, some attempts have been made assuming that the electrons do not lose energy or that scattering cross sections are energy independent; however, no method applicable to more general situations has yet been developed.

[14] L. V. Spencer and U. Fano, J. Research, Natl. Bur. Standards **46**, 446 (1951), where a point-collimated source is also considered. The relation between point and plane isotropic sources is well known from neutron penetration literature.

[15] A word about dimensions: If $I(r,\theta,z)$ has dimensions number per cm^2 per steradian per (g/cm^2) residual range, $N\sigma(r,\Theta)$ being cm^2/g per steradian and r, z being measured in g/cm^2, the first three terms are obviously consistent and the source has the strength (integrated over r, z, Ω) of one electron per cm^2.

[16] H. A. Bethe, *Handbuch der Physik* (Verlag Julius Springer, Berlin, 1933), **24**, Part 1, pp. 491 ff.; Ann. Physik **5**, 325 (1930).

TABLE I. Stopping powers and corresponding residual ranges for electrons calculated from the Bethe formula. The mean ionization potential used is in each case given at the bottom of the column.

	Beryllium		Polystyrene		Air		Aluminum	
Mev	Stopping power $mc^2/(g/cm^2)$	Residual range g/cm^2	Stopping power $mc^2/(g/cm^2)$	Residual range g/cm^2	Stopping power $mc^2/(g/cm^2)$	Residual range g/cm^2	Stopping power $mc^2/(g/cm^2)$	Residual range g/cm^2
0.01	36.83	0.000298	44.55	0.000247	38.80	0.000285	33.25	0.000339
0.03	15.64	0.00211	18.92	0.00175	16.67	0.00199	14.625	0.00230
0.05	10.67	0.00521	12.91	0.00431	11.42	0.00490	10.101	0.00559
0.07	8.402	0.00939	10.17	0.00776	9.011	0.00880	8.008	0.00999
0.10	6.631	0.01734	8.026	0.01514	7.127	0.01619	6.362	0.01830
0.20	4.489	0.05457	5.435	0.04590	4.843	0.05074	4.356	0.05684
0.30	3.780	0.1026	4.576	0.08556	4.087	0.09521	3.690	0.1062
0.40	3.444	0.1571	4.171	0.1306	3.729	0.1456	3.377	0.1619
0.50	3.260	0.2156	3.947	0.1789	3.533	0.1996	3.206	0.2215
0.60	3.150	0.2768	3.814	0.2294	3.417	0.2560	3.105	0.2836
0.70	3.081	0.3397	3.731	0.2813	3.345	0.3139	3.044	0.3473
0.80	3.038	0.4037	3.679	0.3342	3.300	0.3729	3.007	0.4120
0.90	3.011	0.4684	3.646	0.3876	3.272	0.4324	2.985	0.4774
1.00	2.994	0.5336	3.626	0.4415	3.256	0.4924	2.973	0.5431
1.20	2.981	0.6646	3.611	0.5497	3.245	0.6129	2.967	0.6750
1.40	2.984	0.7959	3.614	0.6581	3.250	0.7335	2.975	0.8068
1.60	2.995	0.9269	3.627	0.7662	3.263	0.8537	2.991	0.9380
1.80	3.010	1.057	3.645	0.8738	3.281	0.9733	3.010	1.068
2.00	3.027	1.187	3.666	0.9809	3.301	1.092	3.031	1.198
2.20	3.046	1.316	3.689	1.087	3.323	1.210	3.053	1.327
2.40	3.065	1.444	3.712	1.193	3.345	1.328	3.076	1.454
2.60	3.084	1.571	3.736	1.298	3.367	1.444	3.098	1.581
2.80	3.103	1.698	3.759	1.403	3.389	1.560	3.119	1.707
3.00	3.122	1.824	3.781	1.506	3.410	1.675	3.141	1.832
4.00	3.208	2.442	3.886	2.017	3.508	2.241	3.237	2.446
5.00	3.281	3.045	3.975	2.515	3.591	2.792	3.318	3.043
6.00	3.346	3.635	4.054	3.002	3.664	3.332	3.390	3.626
8.00	3.451	4.786	4.181	3.952	3.783	4.382	3.506	4.760
10.00	3.536	5.906	4.283	4.876	3.878	5.403	3.598	5.862
	$I=60$ ev		$I_H=15.6$ ev $I_C=76.4$ ev		$I_N=80.5$ ev $I_O=92$ ev $I_A=207$ ev		$I=150$ ev	

	Copper		Cadmium		Gold	
Mev	Stopping power $mc^2/(g/cm^2)$	Residual range g/cm^2	Stopping power $mc^2/(g/cm^2)$	Residual range g/cm^2	Stopping power $mc^2/(g/cm^2)$	Residual range g/cm^2
0.01						
0.03	11.91	0.00288				
0.05	8.335	0.00690				
0.07	6.656	0.01220	5.735	0.01433		
0.10	5.323	0.02217	4.610	0.02586	3.926	0.03083
0.20	3.687	0.06791	3.219	0.07842	2.772	0.09214
0.30	3.142	0.1260	2.754	0.1448	2.386	0.1690
0.40	2.886	0.1913	2.538	0.2191	2.206	0.2546
0.50	2.749	0.2609	2.422	0.2982	2.111	0.3455
0.60	2.669	0.3332	2.356	0.3802	2.058	0.4395
0.70	2.622	0.4073	2.318	0.4640	2.028	0.5353
0.80	2.594	0.4823	2.296	0.5489	2.013	0.6322
0.90	2.579	0.5580	2.285	0.6344	2.006	0.7297
1.00	2.572	0.6340	2.281	0.7201	2.004	0.8273
1.20	2.573	0.7862	2.285	0.8916	2.012	1.022
1.40	2.585	0.9381	2.299	1.062	2.027	1.216
1.60	2.602	1.089	2.317	1.232	2.046	1.408
1.80	2.623	1.239	2.337	1.400	2.066	1.599
2.00	2.644	1.387	2.358	1.567	2.087	1.787
2.20	2.666	1.535	2.380	1.732	2.108	1.974
2.40	2.688	1.681	2.401	1.896	2.128	2.158
2.60	2.710	1.826	2.421	2.058	2.148	2.341
2.80	2.731	1.970	2.441	2.219	2.168	2.523
3.00	2.751	2.113	2.461	2.379	2.186	2.703
4.00	2.844	2.812	2.549	3.160		
5.00	2.921	3.491	2.621	3.917		
6.00	2.989	4.153	2.685	4.654		
8.00	3.099	5.437				
10.00	3.186	6.683				
	$I=310$ ev		$I=480$ ev		$I=790$ ev	

following:

$$-\frac{\partial I_{ln}}{\partial t}+S_l(t)I_{ln}(t)=n(2l+1)^{-1}\{(l+1)I_{l+1,n-1}(t)+lI_{l-1,n-1}(t)\}+\delta_{n0}\delta(t-1), \quad (6)$$

where

$$I_{ln}(t)=\int_{-1}^{1}dx x^n I_l(t,x). \quad (7)$$

As discussed in reference 9, formal solutions to Eqs. (6) may be written down. Using these formal solutions, or using Eqs. (6) in much the same manner as in x-ray penetration calculations,[14] the moment coefficients $I_{ln}(t)$ may be determined by numerical integration. However, the selection of numerical methods depends on the behavior of the functions $S_l(t)$. We therefore discuss these functions in the next section and in Appendix A. It turns out from a study of the $S_l(t)$ that other, simpler procedures than straightforward numerical integration may be used to obtain numerically the $I_{ln}(t)$.

3. CROSS SECTIONS

A. Screened Rutherford

The simplest approximate form for the nuclear scattering cross section is the Rutherford formula. For our purposes this cross section should be modified to take into account (a) the screening of the nuclear field by the atomic electrons, (b) deflections caused by inelastic collisions between electrons, and (c) relativistic effects.

As discussed by Bethe,[17] the screening effect may be accounted for by introducing a single parameter. We have chosen to introduce this screening constant η in the Rutherford expression by writing $\frac{1}{4}(1+2\eta-\cos\theta)^{-2}$ in place of the familiar factor $\sec^4(\theta/2)$. In our initial calculations, inelastic deflections were accounted for by means of a multiplicative factor $(Z+1)/Z$. The expression resulting from these modifications is the following:

$$2\pi N\sigma[r(T),\theta]=(3/4)(Z+1)(N_A\phi_0 Z/A)(T+1)^2\times T^{-2}(T+2)^{-2}(1+2\eta-\cos\theta)^{-2}, \quad (8)$$

where the functional relationship between T and r is that of expression (2). In (8), N_A is Avogadro's number, A is the atomic weight, and $\phi_0=(8\pi e^4/3m^2c^4)$. Note that this expression includes relativistic effects insofar as they modify the cross section for very small angles θ. The screening constant η can be determined from the formula of Molière[18]:

$$\eta=\frac{1}{4}\left[\frac{Z^{\frac{1}{3}}}{0.885(137)}\right]^2 T^{-1}(T+2)^{-1}\times[1.13+3.76(Z/137)^2(T+1)^2T^{-1}(T+2)^{-1}]. \quad (9)$$

[17] H. A. Bethe, Phys. Rev. **89**, 1256 (1953).
[18] G. Molière, Z. Naturforsch. **2A**, 133 (1947).

As is discussed in Appendix B, the cross section (8) leads to the following expression for the S_l's:

$$S_l[t(T)]=(Z+1)[3N_A\phi_0 Z/4A]\times(T+1)^2T^{-2}(T+2)^{-2}r_0C_l,$$
$$C_0=0,$$
$$C_1=\ln(1+\eta^{-1})-(1+\eta)^{-1}, \quad (10)$$
$$C_{l+1}=(2+l^{-1})(1+2\eta)C_l-(1+l^{-1})C_{l-1}-(2+l^{-1})(1+\eta)^{-1}.$$

B. Relativistic Forms

Nearly all of our initial calculations were performed by using the expressions (8) and (9). However, a later investigation indicated that if the simple angular dependence of (8) were replaced by the correct relativistic distribution given by the Mott formulas,[19] the S_l's would be modified by as much as 20 percent for large-Z scattering materials at energies as low as $T=1$. Such a modification would markedly affect the electron spatial distributions. It therefore seemed wise to base all further calculations on correct relativistic angular distributions. An investigation of the literature indicated that for some regions of Z and T these have been calculated while for others they apparently have not. Feshbach has made tabulations for a variety of Z's which can be used for $T>8$.[20] For $Z=80$ and a variety of T values, tabulations have been made by Bartlett and Watson[21] and by Massey.[22] For small Z it is possible to use the McKinley-Feshbach expressions.[23] There seem to be no tabulations or formulas approximating the Mott expression for intermediate Z and small T.[24]

A much less important improvement which has nevertheless seemed desirable is that of correcting more accurately for inelastic deflections. This can be done by introducing an additional factor which can be calculated from a formula due to Fano.[25] Although this modification tends to be small, it may be appreciable if Z is low enough.

For calculations in low-Z materials, we use the following expression for the cross section, which relies on the McKinley-Feshbach angular distribution:

$$2\pi N\sigma[r(T),\theta]=(Z+1)(3N_A\phi_0 Z/4A)(1+\epsilon)T^{-1}\times(T+2)^{-1}\beta^{-2}\{(1+2\eta-\cos\theta)^{-2}+2^{-\frac{1}{2}}\pi\alpha\beta(1-\cos\theta)^{-\frac{3}{2}}-\tfrac{1}{2}(\beta^2+\pi\alpha\beta)(1-\cos\theta)^{-1}\},$$
$$\alpha=(Z/137),\quad \beta^2=T(T+2)(T+1)^{-2}, \quad (11)$$

[19] N. F. Mott and H. S. W. Massey, *Theory of Atomic Collisions* (Oxford University Press, London, 1949), second edition, Chap. IV.
[20] H. Feshbach, Phys. Rev. **88**, 295 (1952).
[21] J. H. Bartlett and R. E. Watson, Proc. Am. Acad. Arts Sci. **74**, 53 (1940).
[22] H. S. W. Massey, Proc. Roy. Soc. (London) **A181**, 14 (1942).
[23] W. A. McKinley, Jr., and H. Feshbach, Phys. Rev. **74**, 1759 (1948).
[24] Note that this region is so big that angular distributions change too much to make interpolation feasible.
[25] U. Fano, Phys. Rev. **93**, 117 (1954).

TABLE II. Scattering parameters σ_l as a function of energy. Compare the exact values of columns 2 and 6 with the analytic approximation values in columns 3 and 7. Observe also the constancy of σ_l/σ_1 ratios.

	Aluminum				Gold			
		$\frac{3.193}{r(r+1.492)}$				$\frac{33.93}{r(r+2.086)}$		
Mev	(cm²/g) $N\sigma_1$		σ_2/σ_1	σ_3/σ_1	(cm²/g) $N\sigma_1$		σ_2/σ_1	σ_3/σ_1
2.0	0.9905	0.9907	2.838	5.381	4.902	4.902	2.613	4.631
1.6	1.406	1.401	2.830	5.353	6.948	6.895	2.598	4.581
1.2	2.193	2.183	2.818	5.311	10.80	10.68	2.576	4.512
0.9	3.404	3.396	2.804	5.264	16.64	16.52	2.552	4.436
0.7	4.997	4.998	2.789	5.216	24.18	24.18	2.527	4.363
0.5	8.385	8.413	2.766	5.142	39.77	40.39	2.489	4.254
0.3	18.78	18.82	2.724	5.013	84.78	89.04	2.417	4.056
0.1	127.9	115.5	2.621	4.692	462.3	519.9	2.195	3.440

where, according to Fano,

$$\epsilon=(Z+1)^{-1}(\ln 4\eta)^{-1}\times\{u_{in}-\ln[0.16Z^{-\frac{2}{3}}(1+3.33\alpha/\beta)]\},\quad(12)$$

$-u_{in}$ being a number which differs from one material to the next but which has a value in the neighborhood of 5. The expression for the S_l's which derives from (11) is

$$S_l[t(T)]=(Z+1)(3N_A\phi_0Z/4A)(1+\epsilon)T^{-1}(T+2)^{-1}\beta^{-2}\times\left\{C_l+2\pi\alpha\beta l-(\beta^2+\pi\alpha\beta)\sum_{i=1}^{l}i^{-1}\right\}r_0.\quad(13)$$

For calculations of electron penetration in gold, it proved convenient to represent the cross section by the following expression:

$$2\pi N\sigma[r(T),\theta]=(Z+1)(3N_A\phi_0Z/4A)(1+\epsilon)T^{-1}\times(T+2)^{-1}\beta^{-2}\{(1+2\eta-\cos\theta)^{-2}+B(1-\cos\theta)^{-1}+C+D(1-\cos\theta)\},\quad(14)$$

where B, C, and D are determined so that (14) agrees with the Bartlett-Watson tabulations at appropriate angles. Such a form was found capable of representing the tabulations to 2 percent or better for all angles and all energies. The corresponding formula for the S_l's is

$$S_l[t(T)]=(Z+1)(3N_A\phi_0Z/4A)(1+\epsilon)T^{-1}\times(T+2)^{-1}\beta^{-2}\left\{C_l+2B\sum_{i=1}^{l}i^{-1}+2C(1-\delta_{l0})+2D(1-\delta_{l0}+\tfrac{1}{3}\delta_{l1})\right\}r_0.\quad(15)$$

Both (15) and (13) result from integrals evaluated in Appendix B.

C. Analytic Representations

The expressions (10), (13), and (15) are not simple. However, the S_l's may always be represented with considerable accuracy by the approximate form

$$S_l(t)\approx\alpha d_l/[t(t+\alpha)],\quad(16)$$

where α and d_l are numbers independent of t. The argument which suggested this formula, which was first made by Blanchard[26] and is contained in Appendix A, is not particularly conclusive. However, the accuracy of this representation can be easily demonstrated. For example, it is apparent that (16) holds if the scattering parameters $\sigma_l(r)=\int d\Omega\{1-P_l(\cos\theta)\}\sigma(r,\theta)$ are proportional to $r^{-1}(r+b)^{-1}$, where b is a constant. This, in turn, is the case if $\sigma_1(r)\propto r^{-1}(r+b)^{-1}$ and if the ratios $\sigma_l(r)/\sigma_1(r)$ are independent of r. Table II contains comparisons which demonstrate these proportionalities.

If the source energy is less than about 1 mc^2, an even simpler approximate expression agrees fairly well with the S_l's:

$$S_l(t)\approx d_l/t.\quad(17)$$

This is because the constant α becomes large for low source energies (see Appendix A).

We have used the approximate expressions (16) and (17) in all of our calculations of electron penetration. The discussion contained in the next two sections is based on these representations, which make possible far less laborious methods for the solution of the system (6) than direct numerical or analytical integration.

It should be noted that, as evidenced by Table II, the approximate expressions (16) and (17) are not particularly accurate for $t\ll 1$. This departure becomes somewhat more serious as l becomes larger. This should not particularly affect the accuracy of calculations based on (16) and (17) for several reasons: (a) These discrepancies occur when the electrons have very little of their range and energy left and may be expected to be nearly isotropic in direction. (b) In addition, the scattering cross section for small t becomes large. Thus, the small portion of the electron range where the discrepancy occurs is chiefly spent by the electrons in going around and around rather than in penetrating deeper into the medium. Finally, (c) the fact that the directional distribution of the electrons tends to be isotropic for small t simply means that the higher harmonics, where the discrepancy is larger, are of little importance.

[26] C. H. Blanchard (private communication).

4. CALCULATION OF MOMENTS

We can now discuss methods for calculating the spatial moments $I_{ln}(t)$. The use of the moments once they have been obtained is described in the sections following. For clarity, we relate our discussion mainly to expression (17) for the S_l's. The additional effort involved in using the more general expression (16) is mentioned only at the end of the section, the details being presented in Appendix C.

The formal solution of the differential Eqs. (6) has already been written down by Lewis[7]:

$$I_{ln}(t)=\int_t^1 dt' \exp\left\{-\int_t^{t'} dt''S_l(t'')\right\} \times\{n(2l+1)^{-1}[(l+1)I_{l+1,n-1}(t') +lI_{l-1,n-1}(t')]+\delta_{n0}\delta(1-t')\}. \quad (18)$$

In general, the evaluation of the integrals in (18) must be done numerically. We may estimate the difficulty of such integrations by inserting into (18) the simple form (17) for $S_l(t)$. Use of (17) also makes possible analytic evaluation of at least some of the integrals, this being feasible only for $n\lesssim 4$ because of a rapid increase, with increasing n, in the complexity of the expressions for $I_{ln}(t)$.

With the use of (17), the exponential factor in the integrand of (18) becomes simply $(t'/t)^{d_l}$. As may be seen from Table II, the d_l become large as l increases. Thus the integrand of (18) has a factor which varies rapidly with t. It turns out that the $I_{ln}(t)$ also vary rapidly with t, especially near $t=1$, but in a more complicated manner. The whole integrand therefore varies rapidly with t while not being easily specified analytically. This makes numerical integration a far from trivial problem, especially if values for $I_{ln}(t)$, $n>4$, are desired.

In order to circumvent this difficulty, we investigated the possibility of writing the transport equation in terms of *integrals* of the $I_{ln}(t)$ which would be more tractable for numerical analysis. By dealing directly with the integrals we might also hope to reach more directly the energy dissipation distribution, since this involves integrals rather than the functions $I_{ln}(t)$ directly. The formulation in terms of residual range *moments* may be accomplished very easily, if (17) is used, by simply multiplying Eqs. (6) by a factor t^{p+1} and integrating each term over the whole range $0\leqslant t\leqslant 1$. The result of this operation is the following system of equations:

$$I_{ln}{}^p=\frac{n}{(d_l+p+1)}\left\{\frac{(l+1)}{(2l+1)}I_{l+1,n-1}{}^{p+1} +\frac{l}{(2l+1)}I_{l-1,n-1}{}^{p+1}\right\}+\delta_{n0}(d_l+p+1)^{-1}, \quad (19)$$

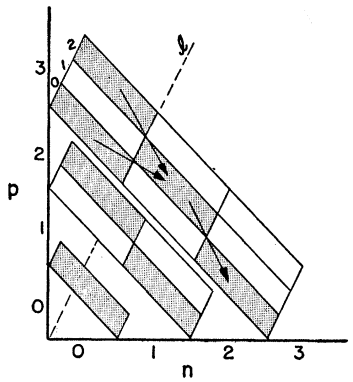

FIG. 1. Diagonal planes and linkages in the lattice of parameters relating to the recursive system (19). The shaded elements can be calculated chainwise as indicated by the arrows.

where

$$I_{ln}{}^p=\int_0^1 dtt^pI_{ln}(t). \quad (20)$$

The linkage between the *numbers* $I_{ln}{}^p$ has a very interesting structure. It obviously can be unraveled, for with $n=0$ the linkage term vanishes and $I_{l0}{}^p=(d_l+p+1)^{-1}$. From these numbers the $I_{l1}{}^p$ may be obtained, which in turn yield the $I_{l2}{}^p$, and so on. If we consider the three dimensional array with sides l, n, and p, all terms in (19) lie in the diagonal plane $(n+p)$ = constant. Further, within this plane the linkage has exactly the triangular structure noted in Fig. 2 of reference 14. Thus, if the elements $I_{ln}{}^p$ are known for fixed n, p and for $l\leqslant l_{\max}$, the elements $I_{l,n+1}{}^{p-1}$ in the next line of the plane may be calculated for $l\leqslant l_{\max}-1$. Since the first line in each diagonal plane, i.e., the line with $n=0$, may be calculated directly, triangular sections of the diagonal planes may be evaluated *independently of all* $I_{ln}{}^p$ *not in the section.* A few such triangular sections are indicated in Fig. 1.

Now the energy dissipation distribution $J(x)$ is given by the integral

$$J(x)=\int_0^1 dt(dT/dt)I_0(t,x). \quad (21)$$

This implies the following expression for the space moments of the energy dissipation distribution:

$$J_n=\int_0^1 dt(dT/dt)I_{0n}(t). \quad (22)$$

If, then, we approximate (dT/dt) by an analytic expression,

$$(dT/dt)\approx A_0t^{-\frac{1}{2}}+A_1t^{\frac{1}{2}}+A_2t^{\frac{3}{2}}, \quad (23)$$

we obtain an expression for the J_n in terms of the $I_{0n}{}^p$:

$$J_n=A_0I_{0n}{}^{-\frac{1}{2}}+A_1I_{0n}{}^{\frac{1}{2}}+A_2I_{0n}{}^{\frac{3}{2}}. \quad (24)$$

The half-integer exponents appear because at low energies $(dT/dt)\propto T^{-1}\propto t^{-\frac{1}{2}}$. We have found (23) to be

capable of representing stopping-power data quite satisfactorily.

Thus, to compute the space moments of the energy dissipation distribution it is necessary to compute elements with half-integer p values within a pyramidal volume in the l, n, p array. Such a calculation is easily accomplished with a desk computer by means of the recursive relations (19), the first ten moments J_n requiring hardly an afternoon's work.

For many problems, and particularly for source energies greater than 1 mc^2, the simple form (17) is not sufficiently accurate and it is necessary to make use of (16). A more involved argument, which is contained in Appendix C, can then be made which yields the following more complicated set of recursive relations:

$$\Phi_{ln}{}^{p}=\frac{\alpha n}{(2l+1)}\sum_{i=0}^{\infty}\frac{(i+1)}{(d_l+p+i+1)}\{(l+1)\Phi_{l+1,\,n-1}{}^{p+i+1}$$
$$+l\Phi_{l-1,\,n-1}{}^{p+i+1}\}+\delta_{n0}\alpha\sum_{i=0}^{\infty}\frac{(i+1)}{(d_l+p+i+1)}(1+\alpha)^{-p-i-1}, \tag{25}$$

where

$$\Phi_{ln}{}^{p}=\int_0^1 dt[t/(t+\alpha)]^{p}I_{ln}(t). \tag{26}$$

The terms in the sums indicated in (25) decrease in size approximately as $(1+\alpha)^{-i}$, while the basic type of linkage remains the same as in the simpler expression (19). In order to calculate moments with the recursive system (25) it is necessary to include enough terms in the calculation to obtain adequate convergence for the more important (smaller) values of p. In a calculation described in Sec. 10 with source energy 1.71 Mev, as many as 25 terms were included to calculate four spatial moments accurately to six significant figures.

A useful device which facilitates the evaluation of the sums in (25) is that of writing, e.g.,

$$\sum_{i=0}^{\infty}\frac{(i+1)}{(d_l+p+i+1)}\Phi_{l+1,\,n-1}{}^{p+i+1}$$
$$=\sum_{i=0}^{\infty}\left\{\sum_{i'=i}^{\infty}(d_l+p+i'+1)^{-1}\Phi_{l+1,\,n-1}{}^{p+i'+1}\right\}. \tag{27}$$

This makes it possible to evaluate simultaneously sums for all values of p for a given l, n combination. Using this device, the illustration just mentioned involving sums with 25 terms required little more than a day's work on a desk computer.

Both (25) and (19) are of a form ideally suited for automatic digital computers. As is mentioned in the next section, some results have been obtained by coding (19) for the SEAC. It is our intention to code (25) as well, in order to perform a wider variety of calculations for energies below 10 Mev. Note that (25) becomes ineffective for source energies above a few Mev because of slow convergence of the sums. For higher energies it may be feasible to use devices for speeding convergence or it may be necessary to derive a different expansion.

Note that in using (25) to obtain the energy dissipation distribution, we write (dT/dt) as a power series similar to (23) but with $[t/(t+\alpha)]$ as independent variable.

5. ASYMPTOTIC CONSIDERATIONS

The process of constructing a distribution from a limited number of moments implies an extrapolation of the moment sequence from the finite number actually calculated to an infinite number of moments. Such an extrapolation can only be done with confidence if the trend of the higher order moments has been established from a knowledge of the distribution near its limits, the so-called asymptotic behavior of the distribution. The determination of this asymptotic behavior requires an independent investigation which is quite different from that leading to the calculation of the spatial moments. Such an investigation has been performed and is to be reported in detail in a manuscript which will be submitted for publication at a later date. In order to make this paper self-contained, a simplified discussion using the method of Wick[11] is contained in Appendix D. Both the simplified and the more detailed arguments indicate that near the $x=1$ limit an analytic behavior similar to the function

$$f(x)=(1-x)^{-\frac{3}{2}}\exp\{-A/(1-x)\} \tag{28}$$

should be anticipated, where A is a constant which depends upon the source energy and the scattering material.

It is conceivable that the spatial distribution attains its asymptotic behavior only very near the limit. In this case knowledge of it could hardly be very useful. Indeed, if a form such as (28) is to prove helpful in constructing a distribution, it should provide a description of the distribution over such a large region of x that those spatial moments which we may be able to calculate reflect this asymptotic behavior. Otherwise our attempts at extrapolating the moment system must contain a large amount of guesswork. It follows that a method for determining the usefulness of a functional form such as (28) is simply to compare the moment trend of (28) with the moment trend of the unknown distribution.

An easily visualized way of making such a comparison is to consider another function with the same asymptotic behavior as (28), namely

$$g(x)=(-\ln x)^{-\frac{3}{2}}\exp\{A/\ln x\}. \tag{29}$$

The equivalence of (29) and (28) for our purpose is easily demonstrated by writing $x=1-(1-x)$ in (29) and expanding around $x=1$. The moments $g_n=$

$\int_0^1 dx x^n g(x)$ are as follows:

$$g_n = (\pi/A)^{\frac{1}{2}} \exp\{-[4A(n+1)]^{\frac{1}{2}}\}. \quad (30)$$

The form of (30) suggests that we plot logarithms of the electron spatial moments *versus* $(n+1)^{\frac{1}{2}}$. A moment trend similar to (30) would be demonstrated by a tendency for the points to lie on a straight line for large n.

A series of such plots is shown in Fig. 2, which utilizes the even spatial moments up to the 20th.[27] The solid lines in this figure were drawn with a straightedge. The circles represent the quantities $-\ln I_{0n}{}^p$ with $p=-\frac{1}{2}$. The fact that the straight line trend holds for moments as low as $n=4$ strongly supports the use of (28) or (29) in representing the unknown distribution.[28]

Having considered the behavior of the electron spatial distribution for $x\rightarrow+1$, a reasonable next step is a discussion of the asymptotic behavior in the other direction, namely for $x\rightarrow-1$. Unfortunately, it is not so easy to establish an analytic law for this backscattered part of the electron distribution. By taking linear combinations of the spatial moments and constructing thereby the sequence $\langle[(1-x)/2]^n\rangle$, which emphasizes the region $x\rightarrow-1$, it is possible to estimate that the behavior resembles the function $\exp\{-A'/(1+x)\}$. This is about the best that can be done at the present time. Fortunately, there is much less interest in the negative x portion of the electron distribution, and moment fitting methods can be used which do not require detailed information about this reverse asymptotic behavior.

6. FURTHER DISCUSSION OF THE DISTRIBUTION

In addition to moments and asymptotic trends, there are a number of other known characteristics which must be taken into account in constructing spatial distributions. The simplest of these are the observations that the distributions should be unimodal and everywhere positive, and that the mode should be located at some positive value of x.

Less obvious characteristics relate to questions of smoothness. It is clear that the distributions should vary smoothly from point to point, without oscillatory or discontinuous behavior, except at the electron source, whose distribution is δ-shaped at $x=0$. The type of discontinuous behavior to be expected at the source can perhaps best be understood by considering the limiting situation of no elastic scattering. In this case, which is closely approximated by heavy particles, electrons generated at $x=0$ would move together through the material to the end of their range. At each point x, all the electrons would have the residual range $t=(1-x)$ and would be dissipating energy at the rate $(dT/dt)_{t=(1-x)}$.

[27] The moment calculations on which Fig. 2 is based were performed with the aid of the SEAC using the screened Rutherford cross section (8) and the simple recursive system (19).

[28] A comparison of moment trends involving (28) rather than (29) can be made, but it is more complicated and less visual.

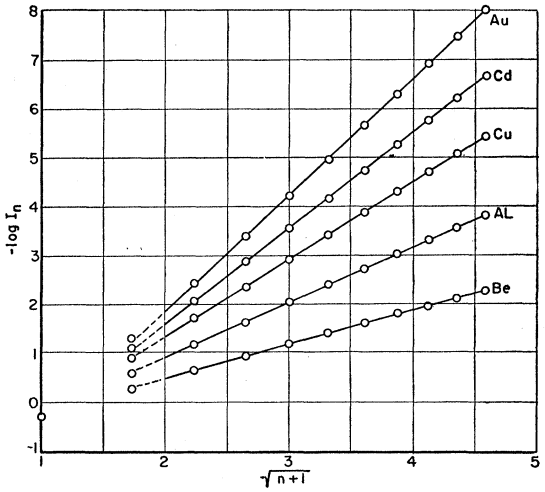

FIG. 2. A graph to demonstrate the asymptotic trend of the moments of electron spatial distributions. The circles represent moments calculated from the recursive system (19). The straight lines represent the trend of Eq. (30).

The energy dissipation distribution starts at $x=0$ with the value $(dT/dt)_{t=1}$; since it vanishes for $x<0$, the source induces a discontinuity of value and slope.[29]

Elastic scattering does not alter the existence or the size of these discontinuities. The distribution of energy dissipation reflects this discontinuous behavior of source energy electrons superposed on the continuous distribution of lower energy electrons, which may be scattered back to the source plane and behind it.

7. CONSTRUCTION OF THE DISTRIBUTION

A. General Discussion

All things considered, the spatial distributions are sufficiently complicated so as to require a fairly large number of constants in their description, i.e., five to ten rather than two or three. For the description must include the backscattering, the discontinuous behavior at $x=0$, the peak, and the asymptotic trend.

By far the best known moment fitting technique which can utilize an arbitrary number of moments is the polynomial method, and in our first attempts to construct spatial distributions we explored its possibilities. After trying it in various forms, e.g., Legendre expansions, expansions based on a weight function specifying the known asymptotic trend, and expansions in non-self-adjoint systems involving only even or odd moments, we finally turned to other methods because the convergence of these expansions was usually poor. The basic reason for this failure seems to be the following: The polynomial method requires the choice of a comparatively simple weight function which so closely estimates the distribution that only minor corrections of a slowly varying nature need to be made in the original estimate. The available quantitative infor-

[29] Note that there are discontinuities in the higher derivatives also, but they need not be considered.

mation about electron spatial distributions is not in a form which allows the selection of such a closely determined, yet simple (i.e., one or two parameter), initial estimate.

Instead of the polynomial method, our chief reliance has been on a "function fitting method."[12] This method has been very successful in problems of x-ray penetration in which information about the distribution is likewise inadequate for a good polynomial weight function.[30] Since it has proven useful, the next few paragraphs are devoted to a general description of it. For *point isotropic* and *plane isotropic* geometry problems, of which there has been little mention thus far in the paper, a different and probably less accurate moment fitting scheme has been used. A description of this latter procedure is contained in the next section.

In the function fitting method the distribution is represented by a sum of terms as follows:

$$J(x)\approx\sum_i a_i F(\beta_i,x). \tag{31}$$

Each term in the sum involves two parameters instead of one as in the polynomial method, and all terms have exactly the same form. The parameters α_i, β_i are determined so that a number of moments of the function on the right agree with moments of the unknown function on the left. This requires the solution of moment equations:

$$J_n=\sum_i a_i F_n(\beta_i). \tag{32}$$

The choice of $F(\beta,x)$ is made according to the following criteria: (a) $F(\beta,x)$ must be capable of describing the asymptotic trend, (b) $F(\beta,x)$ must be simple enough and flexible enough so that a superposition of several terms with different β is capable of describing other known characteristics of the distribution, and (c) $F(\beta,x)$ must have such a form that the Eqs. (32) are easily soluble. This last requirement can always be met if $F_n(\beta_i)$ has the form $(\beta_i)^n\omega_n$, where ω_n is a number independent of β.

The particular selection of $F(\beta,x)$ which has turned out to be most useful is the following:

$$\begin{aligned}F^{(\gamma)}(\beta,x)&=\beta^{-1}(1-x/\beta)^\gamma\exp\{-Ax/(\beta-x)\},\quad 0\leqslant x\leqslant\beta\\&=0,\quad x>\beta,\end{aligned} \tag{33}$$

where γ is a parameter which may be given different values in different problems. Note that with this selection, $\omega_n=\omega_n{}^{(\gamma)}=\int_0^1 dx x^n(1-x)^\gamma\exp\{-Ax/(1-x)\}$. There is some physical basis for this choice of approximating function beyond the selection criteria mentioned in the preceding paragraph. The energy dissipation distribution is obtained by summing the contributions of electrons with different residual ranges. Electrons with residual range t have an asymptotic behavior like that of (33) with $\beta=(1-t)$, as is evidenced, e.g., by expression (67) in Appendix D. Thus the energy dissipation distribution can be written in a form very suggestive of (31), (33).

It may appear surprising that a constant γ is inserted in (33) rather than $-\frac{3}{2}$, which yields precisely the expected asymptotic trend. The reason for this is that the factor $(1-x)^{-\frac{3}{2}}$ has the effect of creating a peak in the approximating function for A not too large. A superposition of several such functions with appreciably different β's must inevitably yield a "bumpy" distribution, which is not acceptable. For the aluminum and gold calculations discussed in Sec. 9, γ was chosen to be zero; while in the beryllium calculation γ was chosen to be $+1$. In each case the selection was made to obtain an approximating function capable of yielding smooth superpositions.

This raises the question as to whether the sum of several such smooth and monotonic functions is capable of producing a distribution which may indeed have a pronounced peak. This is possible, for if two terms in the sum have β's nearly equal and a's which are large and opposite in sign, the behavior of the two combined is similar to that of the function

$$\beta^{-1}(1-x/\beta)^{\gamma-2}\exp\{-Ax/(\beta-x)\}.$$

The choice (33) for $F(\beta,x)$ makes it possible to use the convenient device of fitting separately the even and odd moments. These two sets of moments can be considered as describing two different component distributions which are defined over the range $0\leqslant x\leqslant 1$ and which become asymptotically equal to each other. Each of the two component distributions can be represented by a sum of the form (31). This separate fitting of the even and odd component distributions has several advantages: It considerably simplifies the moment fitting problem, for the component distributions are ordinarily simpler and easier to fit. Further, instead of, say, eight simultaneous equations in the system (32), two systems of four equations each must be solved. The discontinuities at the source plane appear in a harmless and natural form in the component distributions. For example, a discontinuity in the distribution implies that the odd component distribution has a value at $x=0$ equal to the discontinuity size. Likewise, the even component distribution has a finite slope at $x=0$ equal to the (known) slope discontinuity.

Fitting even and odd component distributions separately has one additional advantage, namely it automatically yields an estimate of the accuracy of the approximation. Since the two component distributions become asymptotically the same, differences which appear in the separate constructions must reflect the error. This is important because function fitting techniques have no accompanying test of accuracy comparable with convergence criteria for polynomial approximations. In some cases the use of more and more moments in function fitting construction serves the same purpose, but more frequently the accuracy of

[30] M. Berger (to be published).

construction must be gauged by constructing distributions otherwise known or by comparing constructions based on different functions $F(\beta,x)$.[30]

B. Sample Outline

To illustrate the preceding discussion and to give further details we present here the outline of a typical construction which follows closely the method used for the gold and aluminum calculations of Sec. 9, and which relies on the simple expression (17) for S_l.

(a) First the moments J_n are determined numerically. This requires tabulating stopping powers, evaluating the integral (2) to determine electron residual ranges, calculating the numbers $d_l=S_l(t=1)$ using the appropriate formula for the cross section, computing the quantities $I_{0n}{}^{-\frac{1}{2}}$, $I_{0n}{}^{+\frac{1}{2}}$, and $I_{0n}{}^{\frac{3}{2}}$ from the system (19), and finally combining these quantities as indicated in (24).

(b) Next, the asymptotic constant A in the approximating function (33) must be determined. If moments up to, say $n=10$ have been calculated this is accomplished by solving the equation

$$\ln(J_8/J_{10})=(4A)^{\frac{1}{2}}\{(10.25+A/12)^{\frac{1}{2}}-(8.25+A/12)^{\frac{1}{2}}\}, \quad (34)$$

which corresponds to (70) in Appendix E. A simple iteration is used for this purpose.

(c) We choose $\gamma=0$, noting that the $F^{(0)}(\beta,x)$ superpose smoothly, and calculate the corresponding numbers $\omega_n{}^{(0)}$ with the aid of the formulas developed in Appendix E.

(d) The equations to be solved simultaneously can now be written down. Even and odd component distributions are to be determined separately, requiring the solution of the two systems:

$$\begin{aligned}&\textstyle\sum_i a_i\beta_i{}^n=J_n/\omega_n{}^{(0)}, \quad n=0,\,2,\,4,\,\cdots,\\ &\textstyle\sum_i a_i\beta_i{}^n=J_n/\omega_n{}^{(0)}, \quad n=1,\,3,\,5,\,\cdots.\end{aligned} \quad (35)$$

To the first of these systems we add one more equation which guarantees the known slope change at $x=0$, while to the second (odd) system we add an equation which guarantees the known discontinuity. These two equations are the following:

$$\begin{aligned}&\textstyle\sum_i a_i\beta_i{}^{-2}=A^{-1}(d/dt)(dT/dt)\,|_{t=1},\\ &\textstyle\sum_i a_i\beta_i{}^{-1}=(dT/dt)\,|_{t=1}.\end{aligned} \quad (36)$$

(e) To insure the appropriate asymptotic trend, we specify $\beta_0=1$ in both systems.

(f) To solve each of the two systems, a_0 is first eliminated by subtracting each equation from the succeeding one, i.e., the nth from the $n+2$nd. The resulting system can obviously be put in the form described in Appendix B of reference 12 and the solution proceeds as outlined there.

(g) The resulting even and odd component distributions are combined in the usual manner to obtain $J(x)$.

There is, of course, nothing unique about such a construction. Obvious variations from it are, e.g., use of a different approximating function $F(\beta,x)$, fitting moment combinations instead of the moments directly, solving a single system of equations instead of even and odd components separately, and modifying the moments to make the fitting easier. Such modifications may be desirable at any time and become a necessity in many problems such as, e.g., those in which it is difficult to calculate more than a small number of moments. The unifying feature about such a variety of construction methods is simply that they can all be expected to give similar answers if they express the same quantitative *and* qualitative information about the unknown distribution.[30]

8. PLANE AND POINT ISOTROPIC SOURCES

A. General Discussion

Most of this paper centers around the plane monodirectional source, the geometry of which is easily visualized. Of equal interest and perhaps greater practical importance are the plane and point isotropic sources concerning which an extensive literature exists.[1] The interest in these source types arises because the elementary radioactive source is isotropic.

The distribution resulting from a plane isotropic source may arise in two equivalent situations: (a) Point isotropic sources may be distributed uniformly on a plane. Measurements of the energy dissipated at various distances from the plane may then be made with a point detector. (b) Alternately, the source may actually be point isotropic while the measurement includes all the energy dissipated in a plane layer. If, then, $J^{pl}(|x|)dx$ is the energy dissipated in a plane layer located a perpendicular distance $|x|$ from a point isotropic source, and if $J^{po}(\rho)d\rho$ is the energy dissipated in a spherical shell of radius ρ concentric with the same source, the following relation must hold between the two distributions:

$$J^{pl}(|x|)=\frac{1}{2}\int_{|x|}^{1}\frac{d\rho}{\rho}J^{po}(\rho). \quad (37)$$

Note that x and ρ both measure distance in r_0 units. Multiplying (37) by $|x|^n$ and integrating over the whole range of x yields a corresponding relation between spatial moments

$$J_n{}^{pl}=(n+1)^{-1}J_n{}^{po}, \quad n=0,\,2,\,4,\,\cdots. \quad (38)$$

Because of symmetry all odd moments of the plane distribution vanish. Although odd moments of the point distribution do not vanish they cannot be easily calculated.[14] Thus, it is necessary to rely on even moments in the construction of spatial distributions for both geometries.

The simple relations (37) and (38) make it possible to change from one to the other situation readily. This is very useful, for the plane geometry is much the simpler for the purpose of calculating spatial moments. On the other hand, the point geometry yields spatial distributions which are both easier to discuss and easier to construct. We have therefore always calculated plane moments and then with the aid of (38) constructed distributions for the point geometry which could be transformed to plane distributions by means of (37). This last step has the additional advantage of providing the extra accuracy which accrues to numbers determined by integration.

The recursive systems for obtaining plane isotropic moments can be obtained from (19) and (25) by multiplying the source term by a Kronecker delta factor δ_{l0}, which selects only the isotropic angular component.

The characteristic features of a distribution $J^{po}(\rho)$ resulting from a point source are very similar to those already discussed for the distribution produced by a plane monodirectional source. The asymptotic trend is the same. The discontinuities discussed in Sec. 6 relate to the ordinate and slope of $J^{po}(\rho)$ at $\rho=0$. There is, of course, no backscattered distribution.

The construction of $J^{po}(\rho)$ from its moments and known characteristics can be accomplished by one or another form of the method described in the preceding section. However, we used a simpler (and probably less accurate) method which is described in Part B of this section. Our reasons for choosing this simpler scheme relate to our intention to compare with experiments performed using P^{32} beta rays. The P^{32} spectrum is continuous with an end point at about 1.71 Mev. We therefore decided to construct distributions for a series of monoenergetic sources within the energy region below 1.71 Mev and to integrate over the interpolated results to obtain a distribution relative to the P^{32} source spectrum. Because of the energies involved, most of these monoenergetic source calculations required the more complicated recursive system (25). Since (25) involves more desk computer work than (19), we did not want to calculate so many spatial moments—no more than four, to be precise. On the other hand, the final integration over monoenergetic source results "washes out" the detailed features of each component distribution and is therefore less demanding regarding their accuracy. It therefore seemed appropriate to rely on constructions involving few moments and only fair accuracy.

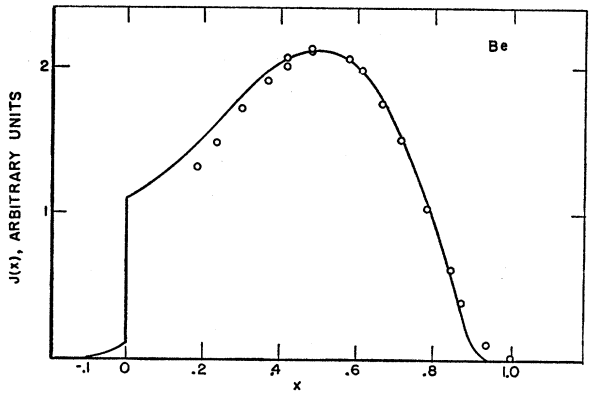

FIG. 3. The energy dissipation distribution resulting from a plane monodirectional source of 500-kev electrons in Be. The circles represent measurements by Frantz which correspond to source electrons with kinetic energy 570 kev. The abscissa is in units of the true range of the source electrons.

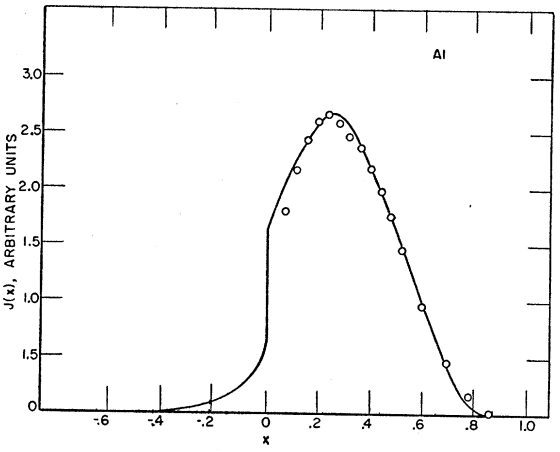

FIG. 4. The energy dissipation distribution resulting from a plane monodirectional source of 500-kev electrons in Al. The circles represent measurements by Frantz corresponding to 515-kev source electrons. The abscissa is in units of the source electron true range.

B. Construction of Distributions

To construct $J^{po}(\rho)$ we decided to use the following function, because of the simple expression for its moments [compare with (29)]:

$$\bar{K}(\rho)=c\rho^{\xi}(-\ln\rho)^{-\frac{3}{2}}\exp\{A/\ln\rho\}, \qquad (39)$$

where c, ξ, A are constants. For $\xi>1$ this function not only vanishes at $\rho=0$ but also has zero slope. We therefore introduce these same characteristics into the distribution to be described by (39) by subtracting from $J^{po}(\rho)$ a function which has the same value and slope at $\rho=0$. This function, which we label $\bar{J}(\rho)$, is so chosen that the combination $J^{po}-\bar{J}$ has the same asymptotic behavior as J^{po} alone. In particular, we used

$$\bar{J}(\rho)=(a+b\rho)\exp\{-B/(1-\rho)\}, \qquad (40)$$

where B is chosen slightly larger than the anticipated value for A, and a, b are adjusted to bring about agreement in slope and value with $J^{po}(\rho)$ at $\rho=0$. The final step in the construction is the determination of the constants c, ξ, A from the solution of equations which guarantee that three moments of $\bar{K}(\rho)$ have values identical with the corresponding moments of

$J^{po}-\bar{J}$. We used for this purpose the zeroth, second, and sixth moments. The fourth moment served as a check on the accuracy of the representation, which has, of course, the form

$$J^{po}(\rho)\approx\bar{K}(\rho)+\bar{J}(\rho). \tag{41}$$

9. EXAMPLES: PLANE MONODIRECTIONAL 500-kev SOURCES IN BE, AL, AND AU

A. Theoretical

These three calculations were performed with the intention of comparing with experiments by Frantz in which the ionization in an air gap is taken as a measure of the energy dissipated.[31] The space-residual range moments $I_{0n}{}^{p}$, which were in each case calculated using the recursive system (19), were therefore combined as in (24) to obtain the J_n but with the constants A_0, A_1, A_2 relative to the stopping power in air in accordance with the Bragg-Gray principle.[32]

The construction of Al and Au spatial distributions followed closely the outline given in Sec. 7, the aluminum moments having been calculated using the $S_l(t)$ given by (13) while the gold moments were obtained using (15) Both constructions involved fitting the moments J_0 through J_7.

The calculation of spatial moments for the distribution in Be made use of (13) and proceeded without difficulty. The construction of the distribution, however, offered special problems. Beryllium has such a low Z that electrons are very little deflected until they have expended an appreciable fraction of their total range. As a result, (a) the asymptotic portion of the distribution is confined to a relatively narrow region of x; (b) the backscattered distribution is very small and tends to fall off rapidly because it is composed largely of very low energy electrons; and (c) the region between source and maximum is large enough to exhibit some structure such as, for example, an inflection. This situation, in which the electron distribution tends to become similar to the Bragg curve for heavy particles, is a fairly general one since it occurs in any scattering material if T_0 is large enough. (Of course, in situations where bremsstrahlung is important, our whole schematization breaks down anyway.)

To construct such a distribution it was not possible to use the same approximating function as for Al and Au, i.e., (33) with $\gamma=0$, because this family of functions does not yield a smooth superposition for small A. Instead, γ was set equal to $+1$ in (33). A corresponding change was made in the unknown distribution, namely $J(x)$ was replaced by $(1-x)J(x)$, so that our approximating function became, in effect, $\{\exp[-Ax/(\beta-x)]\}\times(\beta-x)/(1-x)$, instead of the exponential alone. This change is equivalent to replacing J_n with (J_n-J_{n+1}) in (35).

In treating separately even and odd components as in the sample outline of Sec. 7, it was implicitly assumed that the backscattered part of the distribution blended smoothly with the forward penetrating part. For Be this is not so because the backscattered distribution decreases very rapidly to the left of the source plane. This brings about an additional structure in the component distributions near $x=0$. We made allowance for this by introducing one more term in the sums (35). The contribution of this term is restricted to the region close to $x=0$ by assigning β a small value. To make certain that this additional term described the backscattering, the precise value for β was selected by trial and error so that the corresponding a's determined by the solution of the systems (35) were equal in magnitude and opposite in sign, the even system yielding a positive value.

With these modifications, construction of the Be distribution proceeded satisfactorily. The spatial moments J_0 through J_{10} were used, more being required than for Al and Au because of the use of moment differences and the need to account for additional structure. Had fewer moments been available, our construction would not have depended on the separate construction of even and odd component distributions.

The results of these three calculations are represented in Figs. 3, 4, and 5 by the solid lines. Note the discontinuities, the tremendous increase in the backscattering and the shift of the peak as Z increases, and the similarities between the Be distribution and a Bragg curve for heavy particles.

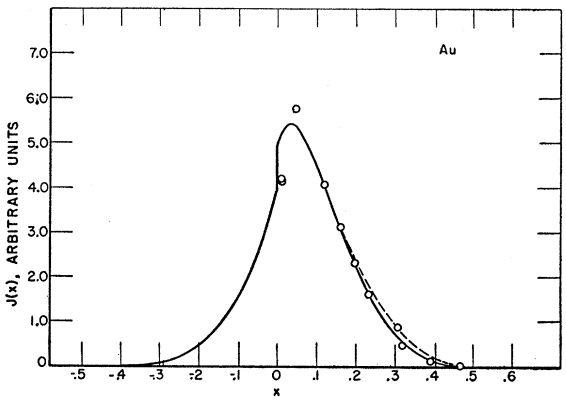

FIG. 5. The energy dissipation distribution resulting from a plane monodirectional source of 500-kev electrons in Au. The circles represent measurements by Frantz corresponding to 495-kev source electrons. The abscissa is in units of the source electron true range. The dashed curve relates to a calculation using the screened Rutherford differential cross section (8) instead of that given by the Mott formula, namely (14).

[31] F. Frantz (private communication).

[32] See L. H. Gray, Proc. Roy. Soc. (London) **A122**, 647 (1929). A more recent theory of cavity ionization takes into account effects neglected in Bragg-Gray theory, namely, those due to the travel of secondary electrons [L. V. Spencer and F. H. Attix (to be submitted for publication)]. We use Bragg-Gray here partly for consistency, since we have nowhere in this paper included secondary electron effects, and partly because changing to a more exact theory of cavity ionization would modify the normalization rather than the distribution shape.

B. Comparison with Experiment

As mentioned at the beginning of this section, F. Frantz has performed experiments which can be compared with the calculated distributions just discussed.[31] Unfortunately, the experimental geometry contained a boundary at $x=0$, so that some features of the comparison are not very meaningful. Still, the influence of the boundary has qualitative significance even at penetrations where it destroys the meaning of a quantitative comparison.

In the Frantz experiments, an accelerator beam of electrons impinged normally on plane foils of the scattering material. Immediately behind these foils was an aluminum-walled ionization chamber. Backing the ionization chamber was a thick slab of the scattering material. The lateral extension of all pieces of the apparatus was effectively infinite, so that the ionization chamber collected all ionization produced in the lateral plane of the air gap. Extrapolation-type measurements were made to verify this point.

Before the electron beam entered the initial foils and the ionization chamber, it passed through an aluminum exit foil on the accelerator tube and several centimeters of air at room pressure. This material, combined with half the ionization chamber thickness, amounted to a total of 15.5 milligrams per cm^2. An allowance for this initial penetration has to be made before comparing measurements with the theory. For measurements of electron penetration in aluminum this could be easily done by considering this initial material to be equivalent to an additional aluminum foil of thickness 15.5 milligrams per cm^2. For measurements in, say, gold a similar but slightly more complicated renormalization was carried out: First the mean cosine of the obliquity distribution resulting from the initial 15.5 mg/cm^2 was calculated. Next we determined the thickness of an equivalent gold foil which would produce the same mean cosine and added this equivalent foil thickness to all penetrations. Finally, the source energy was renormalized so that the mean energy of electrons penetrating the equivalent gold foil corresponded with the mean energy of electrons penetrating the actual initial aluminum-equivalent material.

Unfortunately, the initial penetration made it difficult to perform absolute measurements because of uncertainties in the strength of the initial electron beam. In comparing measurements with theory, the two were matched at a penetration sufficiently great that boundary effects should be negligible but not so great that statistical fluctuations or range straggling effects should be appreciable.

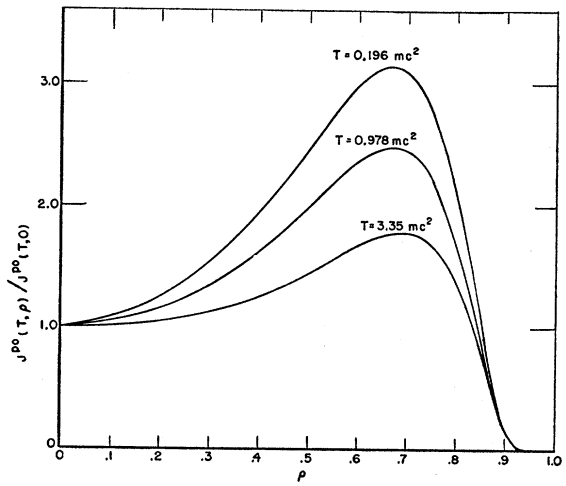

FIG. 6. Energy dissipation distributions resulting from point isotropic sources of monoenergetic electrons in polystyrene. The abscissa gives the penetration in fractions of the source electron true range.

TABLE III. Energy dissipation distributions $[J^{Po}(T_0,\rho)/J^{Po}(T_0,0)]$ resulting from point isotropic sources in air emitting electrons of energy T_0. The symbol ρ represents the distance from the source in units of the initial true range.

ρ	$T_0=0.1$ Mev	0.3 Mev	0.5 Mev	0.7 Mev	1.0 Mev	1.4 Mev	1.71 Mev
0.00	1.000	1.000	1.000	1.000	1.000	1.000	1.000
0.05	1.037	1.025	1.019	1.012	1.010	1.005	1.003
0.10	1.102	1.071	1.055	1.039	1.032	1.021	1.018
0.15	1.196	1.140	1.109	1.083	1.069	1.048	1.037
0.20	1.322	1.235	1.186	1.147	1.122	1.089	1.072
0.25	1.483	1.357	1.287	1.233	1.195	1.147	1.121
0.30	1.670	1.509	1.415	1.343	1.288	1.222	1.186
0.35	1.910	1.690	1.565	1.474	1.400	1.314	1.266
0.40	2.172	1.898	1.739	1.627	1.532	1.424	1.362
0.45	2.454	2.125	1.930	1.798	1.679	1.549	1.473
0.50	2.738	2.357	2.118	1.968	1.827	1.677	1.586
0.55	2.993	2.571	2.288	2.124	1.963	1.798	1.695
0.60	3.174	2.727	2.395	2.227	2.054	1.881	1.771
0.65	3.204	2.764	2.403	2.243	2.077	1.905	1.795
0.70	2.999	2.607	2.230	2.096	1.940	1.802	1.703
0.75	2.362	2.149	1.801	1.714	1.599	1.509	1.438
0.80	1.609	1.447	1.169	1.133	1.070	1.036	1.000
0.85	0.635	0.592	0.452	0.458	0.438	0.443	0.438
0.90	0.066	0.066	0.045	0.056	0.049	0.054	0.057
0.92	0.009	0.013	0.007	0.008	0.009	0.011	0.011

The experimental values, as normalized and corrected for initial penetration, are represented by circles in Figs. 3, 4, and 5. In reducing the experimental penetrations to a scale of $x=z/r_0$, theoretical range-energy curves were used based on data from Table I. The source energies mentioned in the captions are the effective source energies obtained as already described, and the first experimental value gives a measure of the equivalent foil thickness. The question may be raised as to whether it makes sense to compare experimental values with a theoretical curve for a slightly different source energy; however, distribution *shapes* are known experimentally and expected theoretically to be rather independent of source energy particularly for nonrelativistic source energies.[33]

There is good agreement between calculated and

[33] See reference 6 and Fig. 6. Experimental verification of this is due to F. Frantz (private communication).

experimental values in Figs. 3, 4, and 5 except near the source plane $x=0$ and in the extreme tail to the right. Near the source plane, however, boundary effects should produce just such a decrease in experiment relative to theory as is observed, since the absence of the material behind the source plane allows the back-scattered electrons to escape behind the source instead of remaining in its proximity. Likewise, in the tail to the right, range straggling effects not included in the present theory should increase the experimental ionization over that predicted by theory. It is gratifying to note that the range straggling effect seems most serious for beryllium, while the boundary effect is biggest for gold, in agreement with qualitative expectation.

10. FURTHER APPLICATIONS: ISOTROPIC P^{32} SOURCES IN AIR AND POLYSTYRENE

Using methods described in Sec. 8, calculations were performed for isotropic monoenergetic sources in air and in polystyrene, the source energies T_0 being 0.1, 0.3, 0.5, 0.7, 1.0, 1.4, and 1.71 Mev. The 0.1 and 0.3 Mev calculations were accomplished using (19) while all the others used (25). Resulting spatial distributions for point isotropic sources in air are reproduced in Table III. Figure 6 compares similar distributions for several source energies in polystyrene, to illustrate shape changes with changing source energy.

To obtain spatial distributions for the continuous beta ray spectrum of P^{32}, we evaluated the integrals

$$J(s)=\int_s^1 d\tau P(\tau)J^{po}(\tau,s/\tau), \tag{42}$$

where $P(\tau)d\tau$ is the P^{32} source spectrum, i.e., the number of electrons generated with ranges between τ and $\tau+d\tau$, τ being the range relative to that for the 1.71-Mev component, i.e., the spectrum end-point. The parameter s is the radial penetration distance measured in the same units. Our arrangement for evaluating (42) may be of some interest: We changed to the variable $\rho=s/\tau$, i.e., we wrote (42) in the form

$$J(s)=s^{-1}\int_s^1 d\rho\{(s/\rho)^2P(s/\rho)J^{po}(s/\rho,0)\}\times\{J^{po}(s/\rho,\rho)/J^{po}(s/\rho,0)\}. \tag{43}$$

Graphs were then prepared of the slowly varying (with τ) function $\{J^{po}(\tau,\rho)/J^{po}(\tau,0)\}$, which was plotted *vs* τ for fixed values of ρ. Likewise, a graph was prepared of the function $\{\tau^2P(\tau)J^{po}(\tau,0)\}$ plotted against τ. Numbers were read from these graphs for fixed s and evenly spaced ρ values (usually with 0.05 spacing).

To obtain $P(\tau)$, we took a theoretical allowed beta-ray spectrum $P(\eta)$,[34] where η is the electron momentum in mc units, and made the transformation

$$P(\tau)=P(\eta)\frac{d\eta}{d\tau}=P(\eta)\frac{(T+1)}{\eta}(dT/d\tau). \tag{44}$$

Note that $J^{po}(\tau,0)$ is simply the stopping power, so that the first bracketed quantity in (43) contains the square of the stopping power in the factor multiplying $P(\eta)$.

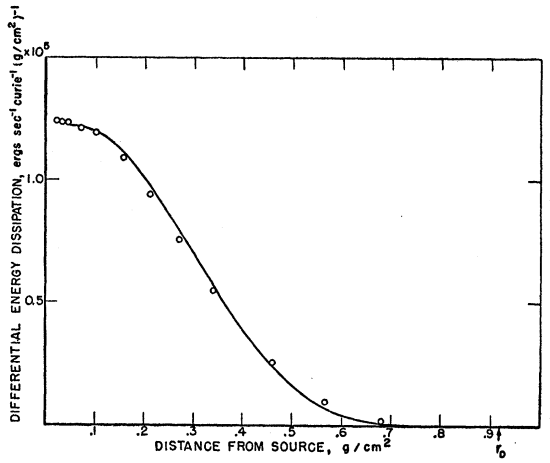

FIG. 7. The energy dissipated in spherical shells around a point isotropic P^{32} beta-ray source in air. The circles represent measurements by Clark, Brar, and Marinelli. Both theory and experiment are given in absolute units.

The P^{32} energy dissipation distributions for point geometry in air and plane geometry in polystyrene are the solid curves in Figs. 7 and 8. The circles in Fig. 7 represent measurements by Clark, Brar, and Marinelli,[35] while the circles in Fig. 8 represent measurements by Loevinger.[1] The theoretical distribution in both cases is given in absolute units. The results of Clark, Brar, and Marinelli given in Fig. 7 are also absolute; however the Loevinger results of Fig. 8 are only relative and were matched with the curve at 0.106 g/cm².

The general agreement is seen to be fairly good except in the tail of the distributions. The plane geometry comparison was put on semilog paper to illustrate the discrepancy which exists for large penetrations. The behavior of this discrepancy is just what would be expected if it were caused by range straggling, which introduces a smear that should increase measurements over theory more and more as the distribution falls more and more rapidly. Correspondingly, since the space integral is not affected by range straggling, the experimental values should fall slightly below theory for small penetrations.

11. REMARKS

The generally good agreement between experiments and the calculations herein described indicates that

[34] The allowed spectrum agrees well with the measurements of beta-ray spectroscopists for this isotope. See, e.g., H. Agnew, Phys. Rev. **77**, 655 (1950), and Sheline, Holtzman, and Fan, Phys. Rev. **83**, 919 (1951).

[35] Clark, Brar, and Marinelli, Radiology **64**, 94 (1955).

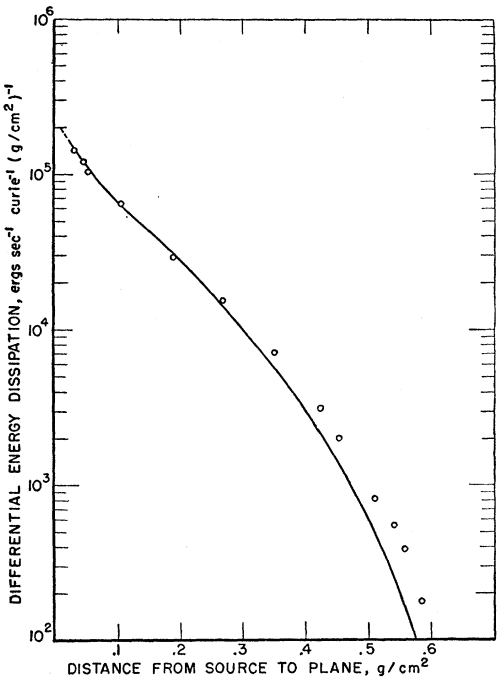

FIG. 8. The energy dissipated in plane layers near a point isotropic P^{32} source in polystyrene. The circles represent measurements by Loevinger. The theoretical curve is given in absolute units; however the experimental values were not absolute and were normalized to agree with theory at 0.106 g/cm².

dependable calculations are possible for all materials and for energies up to a few Mev.

One outstanding defect in the theory is the complete neglect of range straggling. A systematic development of the program outlined in reference 8 would include this effect. The simple degradation problem has already been so treated in reference 7. We intend to complete the theory in this respect.

A desirable extension of this theory would be towards higher energies than a few Mev including, if possible, energy losses due to bremsstrahlung with their inherent magnification of straggling effects.

Finally, it must be emphasized that the whole program undertaken so far is limited to infinite, homogeneous media. The extension of the theory to the treatment of boundary effects, for electrons as well as for x-rays, still represents a major obstacle.

I should like to thank Dr. U. Fano, Dr. C. H. Blanchard, and Dr. M. Berger for many discussions of this material, Dr. Fano again for editorial suggestions, and Miss Ida Hornstein for most of the numerical work involved in preparing tables and graphs.

APPENDIX A

As a first step in constructing an analytic form which may represent with reasonable accuracy the $S_l(t)$ regardless of the source energy, the stopping power must be written in as simple a form as possible. The most obvious simplification to make is that of considering the stopping number B, which is essentially a logarithmic function of the energy, to be a constant. Since the stopping power may be written

$$(dT/dr)=\tfrac{3}{4}(N_A\phi_0 Z/A)B\{1-(T+1)^{-2}\}^{-1}, \quad (45)$$

expression (2) may in the constant stopping number approximation be integrated to yield

$$r(T)=\{3N_A\phi_0 ZB/4A\}^{-1}T^2(T+1)^{-1}. \quad (46)$$

On the other hand, the simplest form to consider for the S_l's is expression (10), which may be written in the form

$$S_l=\tfrac{3}{4}(Z+1)(N_A\phi_0 Z/A)r_0 C_l \times\left\{\frac{(T+1)}{T^2}\right\}\left\{\frac{1}{[T^2/(T+1)]+4}\right\}. \quad (47)$$

If, therefore, we define $\alpha=\{3N_A\phi_0 ZB/4A\}^{-1}4/r_0$, we may rewrite (46) in the form $T^2/(T+1)=4t/\alpha$. Defining $d_l=\frac{1}{4}(Z+1)C_l/B$, it is easily seen that (47) takes the form (16). Further, α increases roughly as T_0^{-2} as the source energy T_0 decreases. Below about 0.5 Mev α is so large that (16) and (17) become equivalent.

This argument hinges on the constancy of α and d_l as the electron energy changes. The energy variation of α is obviously logarithmic. On the other hand C_l and B are both logarithmic functions of the energy, as can be seen from Eq. (10). Thus the energy variation of d_l, which derives from the ratio of these quantities, is slower than logarithmic.

The relativistic modification of the angular distribution of the elastic scattering cross section, which is not included in (47), would seem to disturb the approximate constancy of α and d_l. Fortunately, most of this additional energy dependence is accounted for by simply shifting the values of these constants slightly. Actually, the striking comparisons of Table II were achieved not by the use of theoretical values for these constants but rather by selecting the constants to achieve a good empirical fit to the cross-section tabulation.

APPENDIX B

In order to obtain the S_l expressions (10), (13), and (15) it is necessary to evaluate the integrals

$$\int_{-1}^{1} dy\{1-P_l(y)\}(1+2\eta-y)^{-2},$$

$$\int_{-1}^{1} dy\{1-P_l(y)\}(1-y)^{-q},$$

where $q=\frac{3}{2}$, 1, 0, and -1. The integrals involving the last two values of q are obvious from the orthogonality properties of the P_l and will not be mentioned further.

The integrals $G_l=\int_{-1}^{1}dy\{(1-P_l(y)\}(1-y)^{-1}$ may be evaluated by writing

$$G_{l+1}-G_l=\int_{-1}^{1}\{P_l(y)-P_{l+1}(y)\}(1-y)^{-1}dy.$$

Inserting the familiar Legendre recurrence formula,

$$P_l(y)-P_{l+1}(y)=\frac{1-y}{(l+1)}\{P_{l+1}'(y)+P_l'(y)\},$$

the integration gives the result

$$G_{l+1}-G_l=2(l+1)^{-1}.$$

By induction from the known values $G_0=1$ and $G_1=2$, the final result may be constructed:

$$G_l=2\sum_{i=1}^{l}i^{-1}. \tag{48}$$

In order to evaluate the integral $\int_{-1}^{1}dy\{1-P_l(y)\}\times(1-y)^{-\frac{3}{2}}$, we may start from a generating function for spherical harmonics:

$$\frac{(1-\epsilon^2)}{(1-2y\epsilon+\epsilon^2)^{\frac{1}{2}}}=\sum_{l=0}^{\infty}(2l+1)\epsilon^lP_l(y).$$

By integration, we obtain the equation

$$\int_{-1}^{1}dy\{1-P_l(y)\}(1-2y\epsilon+\epsilon^2)^{-\frac{3}{2}}=\frac{2(1-\epsilon^l)}{1-\epsilon^2}.$$

The limit of this as $\epsilon\longrightarrow 1$ yields the final result:

$$\int_{-1}^{1}dy\{1-P_l(y)\}(1-y)^{-\frac{3}{2}}=2\sqrt{2}l. \tag{49}$$

Finally, the integral

$$C_l=\int_{-1}^{1}dy\{1-P_l(y)\}(1+2\eta-y)^{-2}$$

may be immediately evaluated in terms of Legendre functions of the second kind:

$$C_l=\frac{\partial}{-2\partial(2\eta)}\{Q_0(1+2\eta)-Q_l(1+2\eta)\}. \tag{50}$$

For computation purposes a recursion system may be preferable. This can be easily obtained from the recursion relations between the associated functions Q_l^1. The result is given in (10).

APPENDIX C

In this appendix, the derivation of (25) from (18) and (16) will be sketched. As a first step in this derivation, the terms in (18) are each multiplied by $[t/(t+\alpha)]^p$ and integrated over the range $0<t<1$. Referring to the definition (26), we may write

$$\Phi_{ln}^{p}=\int_0^1 dt[t/(t+\alpha)]^p\exp\left\{-\int_t^1 dt''S_l(t'')\right\}\times\int_t^1 dt'\exp\left\{\int_{t'}^1 dt''S_l(t'')\right\}\times\left\{\frac{n}{(2l+1)}[(l+1)I_{l+1,\,n-1}(t')+lI_{l-1,\,n-1}(t')]+\delta_{n0}\delta(1-t')\right\}. \tag{51}$$

Next, this expression is integrated by parts. Defining

$$L_{lp}(t)=\exp\left\{\int_t^1 dt''S_l(t'')\right\}\int_0^t dt'[t'/(t'+\alpha)]^p\times\exp\left\{-\int_{t'}^1 dt''S_l(t'')\right\}, \tag{52}$$

the expression (51) takes the form

$$\Phi_{ln}^{p}=\int_0^1 dtL_{lp}(t)\frac{n}{(2l+1)}[(l+1)I_{l+1,\,n-1}(t)+lI_{l-1,\,n-1}(t)]+\delta_{n0}L_{lp}(1). \tag{53}$$

The evaluation of the integrals in the exponents of (52) may be accomplished by inserting the analytic form (16):

$$L_{lp}(t)=[t/(t+\alpha)]^p\int_0^t dt'[t'(t+\alpha)/t(t'+\alpha)]^{d_l+p}. \tag{54}$$

The transformation $y=[t'(t+\alpha)/t(t'+\alpha)]$ then leads to the forms

$$L_{lp}=\alpha[t/(t+\alpha)]^{p+1}\int_0^1 dyy^{d_l+p}\left[1-\frac{yt}{t+\alpha}\right]^{-2}=\alpha\sum_{i=0}^{\infty}\frac{(i+1)}{(d_l+p+i+1)}[t/(t+\alpha)]^{p+i+1}. \tag{55}$$

Inserting (55) into (53), we arrive at the recursion system (25).

APPENDIX D

The starting point for an investigation of the asymptotic trend of the electron spatial distribution is a Laplace transformation of Eq. (5). If the terms in Eq. (5) are multiplied by $\exp\{p[x-(1-t)]\}$ and integrated over the range $-\infty<x<(1-t)$, the resulting equation is

$$-\partial F_l/\partial t-\tfrac{1}{2}p\Delta_lF_l+S_l(t)F_l(p,t)=\delta(1-t), \tag{56}$$

where

$$F_l=\int_{-\infty}^{1-t} dx\,\exp\{p[x-(1-t)]\}I_l(x,t) \tag{57}$$

$$\Delta_l F_l=(l+\tfrac{1}{2})^{-1}\{(l+1)(F_{l+1}-F_l)-l(F_l-F_{l-1})\}.$$

The system of Eqs. (56) would be easy to solve were it not for the interlinkage term (57), which requires that all equations be solved simultaneously. Indeed, the different approaches to the problem of obtaining solutions *all* correspond to methods for "breaking through" this interlinkage term. For example, the calculation of moments involves a Taylor series expansion of the F around the point $p=0$. The interlinkage term is then of higher degree in p than the other terms and the equation is solved by iteration starting from zero order in p. Likewise, the familiar diffusion approximation breaks the interlinkage by setting F_2 equal to zero. Unfortunately, as mentioned in reference 2, this predetermines an incorrect asymptotic trend. It also makes no allowance for the tendency of electrons to maintain their original direction during the initial stage of the penetration. As can be seen from Figs. 2–4 there hardly exists a region where distribution of energy dissipation is not dominated either by the asymptotic trend or the initial straight-forward penetration, and thus the diffusion approximation is not applicable to this type of problem.

In the Wick method, the $F_l(p,t)$ are expanded in eigenfunctions of the difference equation

$$-(p/2)\Delta_l\psi(l,p,t)+S_l(t)\psi(l,p,t)=\lambda(p,t)\psi(l,p,t), \tag{58}$$

i.e., we write

$$F_l(p,t)=\textstyle\sum_m a_m(p,t)\psi_m(l,p,t). \tag{59}$$

With this ansatz, (56) becomes

$$-\frac{\partial}{\partial t}\sum_m a_m(p,t)\psi_m(l,p,t)+\sum_m a_m(p,t)\lambda_m(p,t)\psi_m(l,p,t)=\delta(1-t), \tag{60}$$

in which the interlinkage term has disappeared.

Equations for the $a_m(p,t)$ may be obtained by multiplying (60) by $(l+\frac{1}{2})\psi_n(l,p,t)$ and summing over l. Because of the orthogonality of the ψ_m's, the result is

$$-\frac{\partial a_n}{\partial t}-\sum_m{}' M_{nm}(p,t)a_m(p,t)+\lambda_n(p,t)a_n(p,t)=\gamma_n(p)\delta(1-t), \tag{61}$$

where

$$M_{nm}=\sum_{l=0}^{\infty}(l+\tfrac{1}{2})\psi_n\frac{\partial\psi_m}{\partial t} \quad\text{and}\quad \gamma_n=\sum_{l=0}^{\infty}(l+\tfrac{1}{2})\psi_n(l,p,1).$$

The sum in (61) provides a linkage between the a_n's. Due to special scaling properties, this new linkage term in some cases either does not appear or can be shown to vanish in the asymptotic limit of large p. For our purpose the most obvious procedure is an iteration in terms of this linkage. In other words this term is neglected altogether in zeroth approximation. Its effect is then estimated by means of a new calculation in which the linkage term is calculated with the zeroth approximation solutions. Such a calculation has actually been carried out, but its results have been superseded by calculations of a somewhat different type which will be given in a separate paper. We shall carry the calculation here only as far as the zeroth approximation which neglects the interlinkage term altogether. The solutions to (61) are then

$$a_n{}^{(0)}(p,t)=\gamma_n(p)\exp\left\{-\int_t^1 dt'\lambda_n(p,t')\right\}, \tag{62}$$

where the superscript indicates zeroth approximation

This formal expression doesn't mean much until the eigenvalues λ_n have been estimated. Such an estimation is easily performed in the asymptotic limit of large p. (Note that according to (57), if t is fixed and p is large the important values of the quantity $[x-(1-t)]$ tend to be those near zero.) In this case the eigenvalues of the difference equation (58) approach those of the differential equation

$$-\frac{p}{2}\frac{1}{l}\frac{\partial}{\partial l}\frac{\partial}{\partial l}\psi(l,p,t)+\frac{\alpha d}{t(t+\alpha)}l^2\psi(l,p,t)=\lambda(p,t)\psi(l,p,t), \tag{63}$$

where l is now considered a continuous variable. Physically, this means that electrons which have penetrated nearly as far from the source plane as their path length allows must have a directional distribution peaked at $\theta=0$. It is then possible to describe them with an approximation which is accurate for small angles only and which leads to the differential equation (63).[11] Further, form (16) has been used for the $S_l(t)$, with the d_l approximated by dl^2. This approximation describes the directional distribution as a result of a diffusion process, and has been used already by Yang.[11]

Equation (63) is the Schroedinger equation pertaining to a plane oscillator, and its eigenvalues are easily calculated. The following expression for λ_n results:

$$\lambda_n=(n+1)(2\alpha pd)^{\frac{1}{2}}[t(t+\alpha)]^{-\frac{1}{2}}. \tag{64}$$

From this the $a_n{}^{(0)}$ can be obtained:

$$a_n{}^{(0)}=\gamma_n(p)\exp\left\{-p^{\frac{1}{2}}2(n+1)(2\alpha d)^{\frac{1}{2}}\times\ln\left[\frac{1+(1+\alpha)^{\frac{1}{2}}}{\sqrt{t}+(t+\alpha)^{\frac{1}{2}}}\right]\right\}. \tag{65}$$

For large p, the $a_0^{(0)}$ is much larger than the other terms, and the $F_0(p,t)$ is consequently represented by the single term

$$F_0 \sim \gamma_0(p)\psi_0(p,t) \exp\left\{-p^{\frac{1}{2}}(8\alpha d)^{\frac{1}{2}} \ln\left[\frac{1+(1+\alpha)^{\frac{1}{2}}}{t^{\frac{1}{2}}+(t+\alpha)^{\frac{1}{2}}}\right]\right\}. \quad (66)$$

In (66) the p variation of $\gamma_0(p)\psi_0(p,t)$ is so slow that this factor can be considered constant with p. By Laplace inversion of the $F_0(p,t)$, the following form for the electron spectrum is then obtained:

$$I_0(t,x) \sim \gamma_0\psi_0(t)\frac{u(t)}{2\sqrt{\pi}}[(1-t)-x]^{-\frac{3}{2}} \times \exp\left\{-\frac{u^2(t)}{4}[(1-t)-x]^{-1}\right\}, \quad (67)$$

where

$$u(t) = (8\alpha d)^{\frac{1}{2}} \ln\left[\frac{1+(1+\alpha)^{\frac{1}{2}}}{t^{\frac{1}{2}}+(t+\alpha)^{\frac{1}{2}}}\right].$$

The energy dissipation distribution requires an integration over t. For $x \approx 1$, the only contributions to the integral are from the region $t \approx 0$, and the expected asymptotic trend is therefore

$$J(x) \propto (1-x)^{-\frac{3}{2}} \exp\left\{\frac{-u^2(0)}{4(1-x)}\right\}, \quad (68)$$

which has the form (28).

It should be re-emphasized that this derivation is neither complete nor airtight and merely serves here to indicate that the analytic form (28) seems natural to the problem.

APPENDIX E

A useful recursion relation for the moments

$$F_n^{(-\frac{3}{2})} = \int_0^1 dx x^n (1-x)^{-\frac{3}{2}} \exp\{-Ax/(1-x)\}$$

can be obtained from a simple integration by parts:

$$F_n^{(-\frac{3}{2})} = -A\int d\{\exp[-Ax/(1-x)]\}\{x^n(1-x)^{\frac{1}{2}}\}$$
$$= A^{-1}\{nF_{n-1}^{(-\frac{3}{2})} - (2n+\tfrac{1}{2})F_n^{(-\frac{3}{2})} + (n+\tfrac{1}{2})F_{n+1}^{(-\frac{3}{2})}\}, \quad n>0$$
$$= (\pi/A)^{\frac{1}{2}}e^A \operatorname{Erfc}((2A)^{\frac{1}{2}}), \quad n=0. \quad (69)$$

Unfortunately, higher moments can be calculated in this way only at the expense of accuracy. It is therefore necessary to develop an expression which is asymptotically accurate for the high order moments. This can be done by means of the transformation $x=\exp(-y)$:

$$F_n^{(-\frac{3}{2})} = \int_0^\infty dy e^{-(n+1)y} \exp\{-A(e^y-1)^{-1} - \tfrac{3}{2}\ln(1-e^{-y})\}.$$

Since large n implies that the important contributions to the integral come from small y, the bracketed term is now expanded in powers of y. The result of retaining powers up to the first is as follows:

$$F_n^{(-\frac{3}{2})} \approx e^{A/2}\int_0^\infty dy y^{-\frac{3}{2}} \exp\{-(n+\tfrac{1}{4}+A/12)y - A/y\}$$
$$\approx (\pi/A)^{\frac{1}{2}}e^{A/2} \exp\{-[4A(n+\tfrac{1}{4}+A/12)]^{\frac{1}{2}}\}. \quad (70)$$

This is the desired asymptotic expression.

In the same way, a similar recursion expression can be written for the moments $F_n^{(0)}$:

$$F_n^{(0)} = A^{-1}\{nF_{n-1}^{(0)} - 2(n+1)F_n^{(0)} + (n+2)F_{n+1}^{(0)}\}$$
$$= 1 - Ae^A\{-\operatorname{Ei}(-A)\}, \quad (71)$$

and also an asymptotically correct expression for large n:

$$F_n^{(0)} \approx (n+1+A/12)^{-1}e^{A/2}L_1[4A(n+1+A/12)]^{\frac{1}{2}},$$
$$L_1(y) = yK_1(y). \quad (72)$$

In calculating moments, particularly for large A, we have found it convenient to use the asymptotic expression to obtain two successive large moments, say $n=20, 21$. Lower moments are obtained by working the recursion expression (69) or (71) backwards. All moments are then slightly readjusted so that $F_0^{(0)}$ agrees with the value calculated from expression (69) or (71).